



Intolerance of uncertainty modulates brain-to-brain synchrony during politically polarized perception

Jeroen M. van Baar^a, David J. Halpern^{b,c}, and Oriel FeldmanHall^{a,d,1}

^aDepartment of Cognitive, Linguistic, and Psychological Sciences, Brown University, Providence, RI 02912; ^bDepartment of Psychology, New York University, New York, NY 10002; ^cDepartment of Psychology, University of Pennsylvania, Philadelphia, PA 19104; and ^dCarney Institute for Brain Science, Brown University, Providence, RI 02912

Edited by Rose McDermott, Brown University, Providence, RI, and accepted by Editorial Board Member Michael S. Gazzaniga April 8, 2021 (received for review November 25, 2020)

Political partisans see the world through an ideologically biased lens. What drives political polarization? Although it has been posited that polarization arises because of an inability to tolerate uncertainty and a need to hold predictable beliefs about the world, evidence for this hypothesis remains elusive. We examined the relationship between uncertainty tolerance and political polarization using a combination of brain-to-brain synchrony and intersubject representational similarity analysis, which measured committed liberals' and conservatives' ($n = 44$) subjective interpretation of naturalistic political video material. Shared ideology between participants increased neural synchrony throughout the brain during a polarizing political debate filled with provocative language but not during a neutrally worded news clip on polarized topics or a nonpolitical documentary. During the political debate, neural synchrony in mentalizing and valuation networks was modulated by one's aversion to uncertainty: Uncertainty-intolerant individuals experienced greater brain-to-brain synchrony with politically like-minded peers and lower synchrony with political opponents—an effect observed for liberals and conservatives alike. Moreover, the greater the neural synchrony between committed partisans, the more likely that two individuals formed similar, polarized attitudes about the debate. These results suggest that uncertainty attitudes gate the shared neural processing of political narratives, thereby fueling polarized attitude formation about hot-button issues.

political polarization | intolerance of uncertainty | brain-to-brain synchrony | intersubject representational similarity analysis

Countries around the world are experiencing the strain of growing political polarization (1–5). Opposing partisans come to see the world through different eyes. Where one sees the freedom to choose, another sees murder; where one sees the right to protest, another sees violent conduct (6–8). Such a polarized perception of reality hampers bipartisan cooperation and can even undermine the basic principles of democracy (8, 9).

How does polarization arise? One popular theory posits that a need to have certain, structured, and stable beliefs about the world drives people toward political extremes (10–13). Rather than seeing the world in nuanced shades of gray, cognitively rigid individuals perceive information in black and white, painting the world in categorical and predictable terms (14)—a view that dovetails with the immutable taxonomy of political ideologues (15–19). The rigid mind is characterized by a trait-like tendency to find unpredictable and uncertain events aversive and threatening (14, 20, 21) and has long been theorized to play an outsized role in shaping polarized perceptions (22–26). Although recent work suggests that uncertainty can impact the evaluation of political candidates (27) and policy positions (28, 29) and is a major factor contributing to political conservatism (30, 31), the link between uncertainty and political polarization remains unclear. Here, we examine whether individual differences in intolerance of uncertainty (IUS) (20, 21) shape how naturalistic political information is processed in the brain at the time of perception. We test the hypothesis that uncertainty-intolerant individuals interpret

polarizing political information through an ideologically biased, subjective “lens” that produces clear-cut judgments of the issue at hand (20, 32). We further examine whether the neural fingerprint of these uncertainty-driven polarized perceptions—that is, increased brain-to-brain synchrony between like-minded partisans—predicts the formation of polarized attitudes.

We combine two techniques to measure polarized perceptions of political information. First, intersubject correlation [ISC (33)] provides a direct measure of the similarity in subjective interpretations of naturalistic social stimuli (e.g., video narratives) among participants (34, 35). This technique capitalizes on the neural processes triggered by incoming auditory and visual information. If two individuals exhibit similar neural profiles when processing the same incoming information (e.g., synchronized blood oxygen level-dependent [BOLD] responses in functional MRI [fMRI]), they likely have a shared perception and understanding of that information (36–40). Given that ISC offers an established metric to gauge whether individuals are processing information in a similar way, we can use it to test whether two individuals who share the same political ideology also have similar subjective perceptions of political information, which circumvents issues with demand characteristics and explicit self-report (41). Second, to make neural synchrony analyses sensitive to more subtle differences along the ideological continuum than simple left–right groupings and to test for interactive effects between ideology and intolerance to uncertainty, we combine ISC with intersubject representational similarity analysis

Significance

Political partisans view the world through a biased lens, but little is known about how these biased perceptions of reality arise. We measured the brain activity of committed partisans watching real political video footage. Although all participants viewed the same videos, brain responses diverged between liberals and conservatives, reflecting differences in the subjective interpretation of the footage. This polarized perception was exacerbated by a personality trait: intolerance of uncertainty. Participants less tolerant to uncertainty in daily life had more ideologically polarized brain responses than those who tolerate uncertainty. This was observed on both sides of the ideological aisle. This suggests that aversion to uncertainty governs how the brain processes political information to form black-and-white interpretations of inflammatory political content.

Author contributions: J.M.v.B. and O.F.H. designed research; J.M.v.B. performed research; J.M.v.B. and D.J.H. contributed new reagents/analytic tools; J.M.v.B. and D.J.H. analyzed data; and J.M.v.B. and O.F.H. wrote the paper.

The authors declare no competing interest.

This article is a PNAS Direct Submission. R.M. is a guest editor invited by the Editorial Board.

Published under the PNAS license.

¹To whom correspondence may be addressed. Email: oriel.feldmanhall@brown.edu.

This article contains supporting information online at <https://www.pnas.org/lookup/suppl/doi:10.1073/pnas.2022491118/-DCSupplemental>.

Published May 13, 2021.

[IS-RSA (42–44)]. This versatile approach enables us to leverage continuous individual differences and test whether uncertainty attitudes exacerbate the processing of political information in the brain to fuel polarized political attitude formation.

Using a combination of targeted online and field recruiting ($n = 360$), we invited 22 liberals and 22 conservatives to participate in a study on political cognition (Fig. 1A). While undergoing fMRI, participants viewed three types of videos: a neutrally worded news segment on a politically charged topic (abortion; taken from Public Broadcasting Service [PBS] News), an inflammatory debate segment (police brutality and immigration; taken from the 2016 Cable News Network [CNN] Vice-Presidential debate), and a nonpolitical nature video (taken from British Broadcasting Corporation [BBC] Earth; Fig. 1B). Neural data analysis consisted of time locking the fMRI BOLD signal to the onset of the videos and computing voxel-wise time course correlations between each possible pairing of subjects across the entire participant pool, resulting in a “neural synchrony” measurement that indexes shared subjective interpretations of dynamic, naturalistic stimuli (35, 45, 46). We first analyzed behavioral responses to the videos to test whether ideology, IUS, or both predicted similarities in attitude formation about the presented political videos. Next, we analyzed variation in neural synchrony across participant dyads using IS-RSA (Fig. 1D)

to test three interrelated hypotheses: 1) shared ideology between subjects will predict brain-to-brain synchrony during the perception of political stimuli, 2) IUS will modulate this neural synchrony in committed partisans, and 3) increasing neural synchrony will predict the subsequent expression of shared polarized attitudes about the political stimuli.

Results

Behavioral Results: Ideology Predicts Attitudes about Political Videos.

We first confirmed the ideological opposition of our participants by testing whether the two political videos yielded different judgments from our liberal and conservative participants. All participants rated their agreement with several statements made during the videos, such as “The immigration reform plan of Hillary Clinton and Tim Kaine amounts to amnesty” (CNN vice-presidential debate) on a scale from -4 (strongly disagree) to $+4$ (strongly agree). We computed intersubject agreement about a given video between all possible pairings of subjects (dyads) as the cosine similarity between the two participants’ ratings. We then tested whether this intersubject agreement score was significantly greater for pairs of participants who shared a similar political ideology than for dyads with different ideologies. Participants reported their political ideology using a slider (47) ranging from

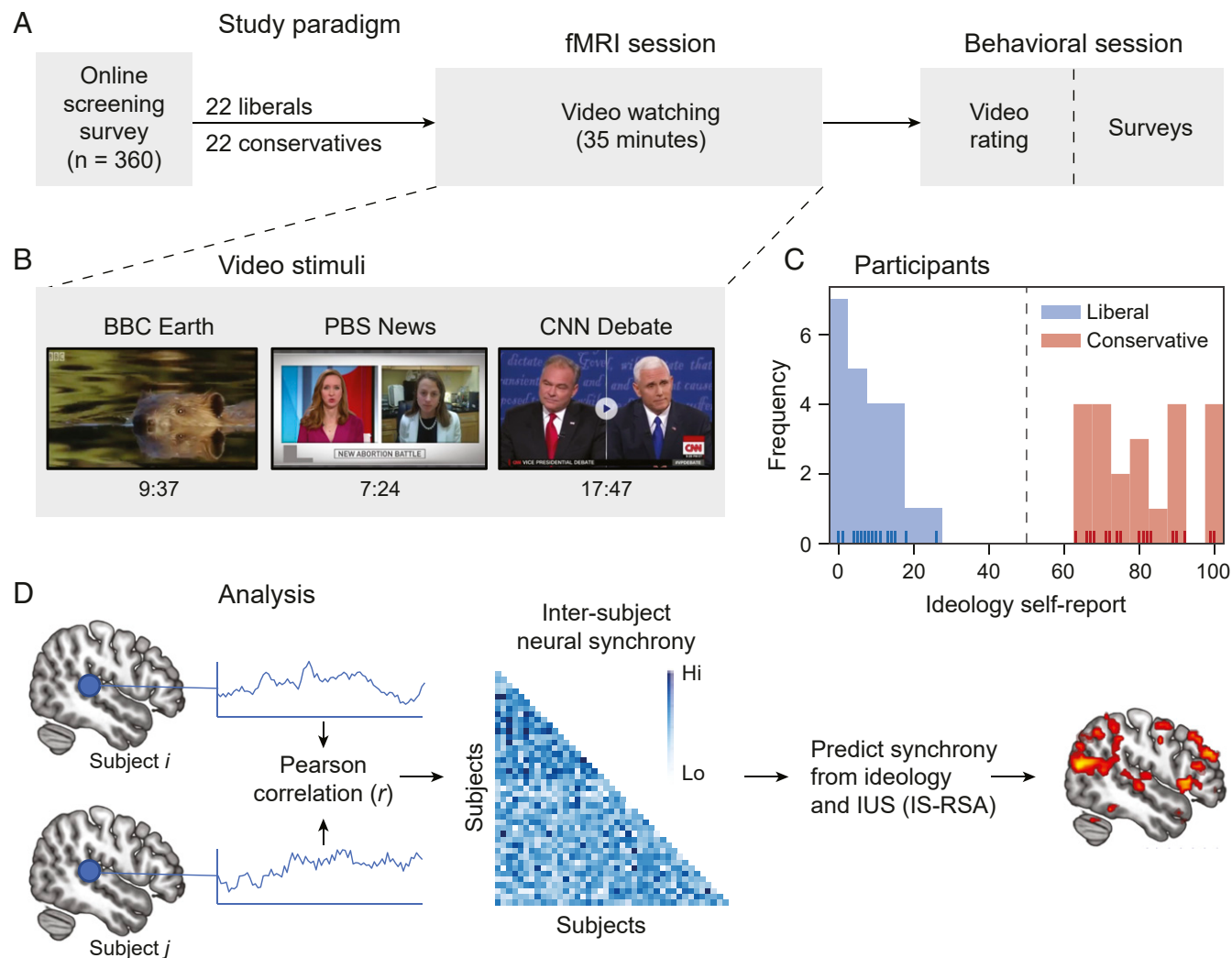


Fig. 1. (A) Participants underwent fMRI and behavioral testing as part of a larger study on political cognition. (B) Participants viewed three videos in a fixed order while undergoing fMRI. (C) Participants were clearly divided on political ideology. (D) Analytical approach. We tested for variation in neural synchrony as a function of ideology and IUS. The statistical map slice is taken from Fig. 2C.

“extremely liberal” (0) to “extremely conservative” (100; Fig. 1C; see Methods for validation). How closely two participants’ ideologies matched up served as a predictor of intersubject judgment similarity in a dyadic regression model (i.e., a regression in which each observation describes the similarity between a pair of subjects), which accounts for inherent statistical dependencies between dyads using linear mixed-effects modeling (42). This regression-based IS-RSA allows us to 1) directly test relationships between distinct data sources (48), including individual differences (e.g., ideology), behavioral responses (e.g., video judgment), and neural activity, and 2) evaluate hypotheses about the interactions between several predictors simultaneously (e.g., ideology and IUS scale), which is not possible in standard RSA approaches in which one behavioral measure predicts neural activity pattern similarity.

Unsurprisingly, the results revealed that ideological similarity robustly predicts holding similar attitudes about both the abortion [$\beta = 0.538 \pm 0.076$ (SE), $t(830.7) = 7.1$, $P < 0.001$] and debate videos [$\beta = 0.847 \pm 0.047$ (SE), $t(824.5) = 18.0$, $P < 0.001$]. This effect was amplified for the vice-presidential debate, for which we observed significantly more polarized attitudes compared to the neutrally worded abortion video [interaction between ideological similarity and video condition: $\beta = 0.310 \pm 0.089$ (SE), $t(1664.3) = 3.48$, $P < 0.001$]. We next evaluated whether intolerance to uncertainty—assessed with the well-validated, 27-item IUS, which includes items like “The ambiguities in life stress me” (21)—could account for this effect. Although intolerance to uncertainty has been linked with extremism, we did not observe any correlation between IUS and ideology [$r(41) = -0.14$, $P = 0.35$] or extremism [distance from the ideology scale midpoint; $r(41) = -0.06$, $P = 0.69$], allowing us to test for independent effects of ideology and IUS on neural synchrony.

Ideological Similarity Drives Neural Synchrony during Political Videos.

After running a standard manipulation check to ensure that our stimuli elicited robust neural synchrony between all participants [SI Appendix, Fig. S1 (34)], we tested whether ideological similarity drives brain-to-brain synchrony. To this end, we computed intersubject ideological similarity as $100 - |ideology_i - ideology_j|$, z-scored this metric, and used this as a predictor of neural synchrony in our dyadic regression IS-RSA model. This revealed no significant clusters for the BBC Earth video, only right angular gyrus involvement for the neutrally worded PBS News abortion segment, and many clusters for the political debate video, in which shared ideology was predictive of a more globally synchronized brain response (Fig. 2A–C). Active clusters for the debate video included regions associated with valuation [ventral striatum and orbitofrontal cortex (OFC) (49, 50)], theory of mind [temporoparietal junction (TPJ) and precuneus (51)], and affect [OFC and anterior insula (AI) (52, 53)]. Even though abortion is a highly polarizing topic, the neutrally worded news video yielded much less ideology-driven neural synchrony than the inflammatory debate video, mirroring the behavioral results. This suggests that polarized perception is not just driven by ideological differences but also by the way polarizing issues are presented. Moreover, individual subject time courses in medial OFC (mOFC; Fig. 2D) suggest that the BOLD signal was synchronized between like-minded individuals, regardless of whether they were both liberal or both conservative, a hypothesis which we formally test below.

Intolerance of Uncertainty Exacerbates Ideology-Driven Neural Synchrony.

We then turned to our main question about whether uncertainty attitudes shape polarized information processing in the brain. By linking neural synchrony to IUS, we could test our key hypothesis that participant pairs with similar political views would have even greater neural synchrony if they were also uncertainty intolerant. We first defined a pairwise metric of “joint IUS” as the product of the two IUS scores for each dyad and interacted this predictor

with ideological similarity in our IS-RSA model of neural synchrony during the debate video. Confirming our hypothesis, the ideology–IUS interaction strongly predicted neural synchrony over and above ideological similarity in 10 clusters of voxels (Fig. 3A and SI Appendix, Fig. S2 and Table S1). Five of these clusters were located in regions associated with mentalizing, valuation, and emotion, namely, bilateral TPJ, precuneus (two clusters), and right OFC, extending into the AI, which were also preregistered regions of interest for this study. These regions have been implicated in cognitive functions that align with the polarized processing of information, including the understanding of shared narratives [TPJ and precuneus (54–58)], valuation [OFC (50, 53, 59)], and affect [OFC/AI (52, 53, 59–61)]. The remaining five clusters were in regions functionally associated with the processing of eye movements (frontal eye fields; three clusters) and visual motion (middle temporal area; two clusters), possibly reflecting differences in visual search during political information processing (62). Although IUS was correlated with another questionnaire that taps into mental rigidity (i.e., need for closure [NFC]) in our dataset, joint NFC did not interact with ideology to predict neural synchrony (SI Appendix, Supplementary Results).

To understand the directionality of the observed ideology–IUS interaction effects, we plotted the neural synchrony predicted by the fitted regression models in the regions involved in higher-order cognition, which included TPJ, OFC, and precuneus (Fig. 3B and C and SI Appendix, Table S3). For each of these regions of interests (ROIs), intolerance to uncertainty exacerbated neural polarization, such that two individuals who were both intolerant to uncertainty and similar in ideology produced significantly more neural synchrony.

Intolerance of Uncertainty Modulates Neural Synchrony among Liberals and Conservatives.

To formally test whether intolerance to uncertainty affected ideological processing writ large or was restricted to one side of the political spectrum, we modified the regression by replacing the “ideology similarity” predictor with a categorical predictor called “ideology pair.” This reflects how the political spectrum is typically dichotomized into a liberal and a conservative (CL) pole and allows us to investigate whether the observed neural synchrony effects also arise as a function of political group membership. Effectively, this analysis examines whether there is evidence of neural synchrony within liberal and conservative dyads relative to dyads containing one liberal and one conservative. The categorical ideology pair predictor is then interacted with the continuous joint IUS predictor. The resulting analysis of covariance (ANCOVA) corroborates our results reported with fully continuous predictors: At the omnibus level, there were 19 significant regions of the brain which mostly overlapped with the regions found for the continuous ideology–IUS interaction (SI Appendix, Fig. S3A and Table S2), although we additionally find activity in the bilateral dorsomedial prefrontal cortex (DMPFC), which dovetails with recent research implicating neural synchrony differences in this region between groups of opposing partisans (34).

Critically, post hoc pairwise comparisons showed that the IUS-dependent change in neural synchrony was present for both liberal and conservative dyads in two brain regions that play key roles in value (50, 59), emotion (60, 61), and perspective taking (54–58): right OFC (rOFC; extending into AI) and right TPJ (SI Appendix, Fig. S3B and Table S4). In these regions, which overlapped with the clusters obtained in the continuous ideology–IUS interaction, increased IUS predicted an increase in neural synchrony if two participants belonged to the same ideological pole and a decrease in neural synchrony between pairs with one liberal and one conservative. Put simply, biased information processing in key regions of interest was not unique to any particular political persuasion but rather affected uncertainty-intolerant partisans across the board.

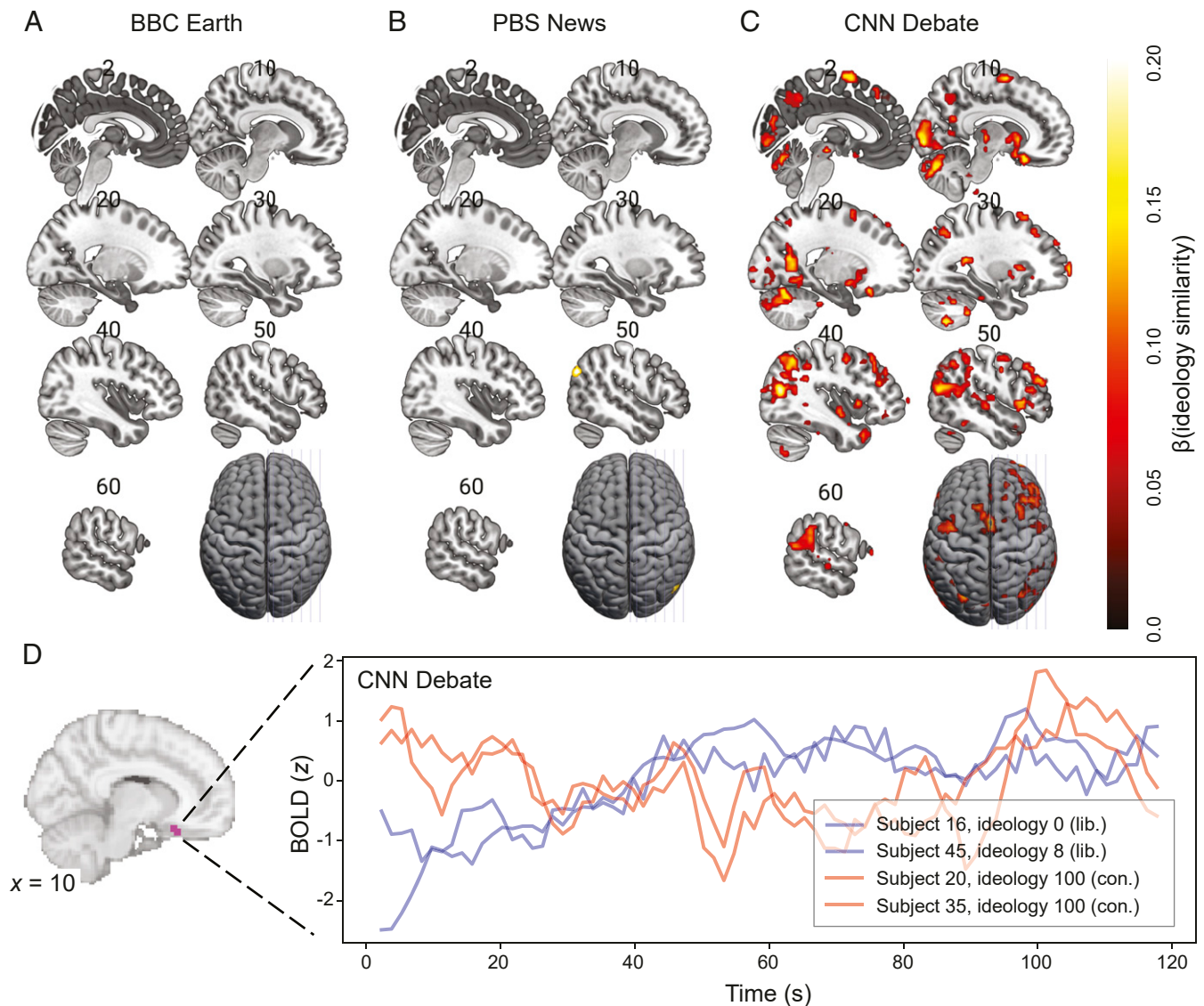


Fig. 2. (A–C) Ideology similarity drove the greatest brain-to-brain synchrony during an inflammatory political debate video (C). Statistical thresholds: voxel-wise P (FDR) < 0.05, cluster size ≥ 5 voxels (135 mm³). Slice numbers indicate MNI x coordinate. (D) Activity time courses in mOFC were synchronized between like-minded individuals. Representative pairs of subjects exhibiting neural synchrony in the mOFC are presented for the first 2 min of video 3, during which liberal Democrat Tim Kaine is speaking. BOLD is z-scored at the subject level; time courses are smoothed using a 6-s rolling window average to reveal trends at the intrinsic timescale of the BOLD response.

Neural Synchrony Predicts Postscan Polarized Attitude Formation.

How might neural synchrony during naturalistic political information processing influence behavior? If similarities in neural processing reflect similarities in the subjective experience of the information, then neural synchrony should predict post hoc judgments about the presented video material. To probe whether brain-to-brain synchrony indeed predicted the subjective interpretation of narrative information (35, 40), leading to politically relevant judgements, we extracted the average fMRI BOLD signal from the mentalizing and emotion brain regions where we found a significant interaction effect of ideology and IUS on neural synchrony (i.e., bilateral TPJ, precuneus, and right OFC extending into AI). For each of these ROIs, we took the neural synchrony between each pair of participants and added this similarity metric to a dyadic regression model that already contained predictors for ideology similarity, joint IUS, and the ideology–IUS interaction. We then used this model to predict judgments about the debate. We found that ROI-wise neural synchrony was a

significant predictor of judgment similarity in rOFC [synchrony predictor: $\beta = 0.048 \pm 0.019$ (SE), t (846) = 2.52, $P = 0.006$; a trend was observed in the two precuneus clusters: $\beta = 0.041 \pm 0.026$ (SE), t (769) = 1.60, $P = 0.055$; $\beta = 0.027 \pm 0.018$, t (840) = 1.46, $P = 0.072$]. When removing neural synchrony from the model, joint IUS did not significantly interact with ideological similarity to predict intersubject judgment similarity for either video [abortion video: $\beta = -0.305 \pm 0.364$ (SE), t (831.8) = -0.837, $P = 0.40$; debate video: $\beta = -0.234 \pm 0.226$ (SE), t (825.1) = -1.03, $P = 0.30$]. Together, these results reveal a system in which ideology and IUS interact to shape neural synchrony, which in turn drives similarities in political judgment. This suggests that uncertainty-driven neural polarization plays a mechanistic role in the formation of polarized political attitudes.

Discussion

Political polarization afflicts many countries (1–5), manifesting in ideologically biased perceptions of the same political reality

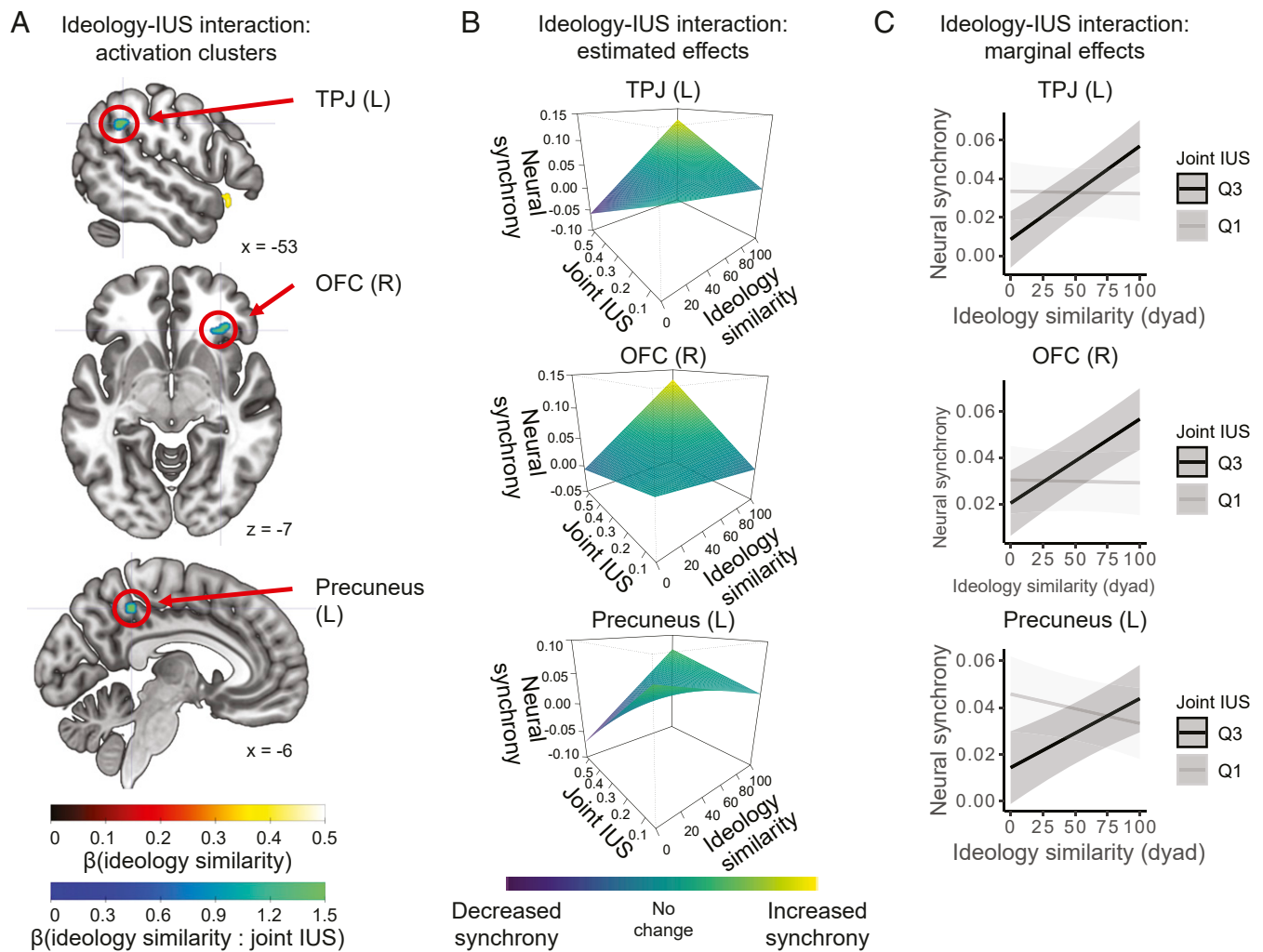


Fig. 3. (A) Neural synchrony in key socioemotional brain regions was driven by the interaction between uncertainty intolerance (IUS) and ideology. Thresholds: voxel-wise P (FDR) < 0.05 and cluster size ≥ 5 voxels (135 mm³). (B) Simulating neural synchrony from the regression model (with unstandardized ideology similarity to illustrate the effect) revealed that joint IUS exacerbated neural polarization: The ideological similarity of a dyad (continuous) more strongly predicted neural synchrony when participants were intolerant to uncertainty (high in joint IUS). (C) Estimated marginal effects for neural synchrony by joint IUS (lower quartile, Q1, and upper quartile, Q3) confirmed this interpretation: High IUS boosted neural synchrony in participant pairs with similar ideology (high-ideology similarity) and lowered synchrony for ideologically opposed dyads (low-ideology similarity). Shaded zones represent 95% CIs. Regression coefficients are reported in *SI Appendix, Table S3*.

(6–9). The polarized mind can be traced to social identity theory (63, 64), which posits that individuals swiftly identify with other seemingly like-minded individuals, yielding a heated tribalism plagued by “Us versus Them” mentalities (65, 66). Although it is critical to understand how political polarized perceptions arise and lead to widespread negative evaluations of the political outgroup (67–69), the neurobiological mechanisms governing this process remain largely unknown (4, 70). Research illustrates that holding polarized beliefs satisfies a need for certain and stable perspectives about the world, which accords with popular psychological theories that an aversion to uncertainty plays a critical role in driving political polarization (11, 25, 30). Leveraging a brain-to-brain synchrony analysis, we tested whether uncertainty intolerance modulates synchronized BOLD signal in similar-minded partisans watching a political debate.

Our findings are threefold. First, increased neural synchrony was observed among committed partisans on each side of the ideological divide, revealing that sharing strong partisan beliefs—regardless of political affiliation—yield polarized neural encoding of a political stimulus at the time of perception. Second, uncertainty aversion

exacerbated this effect, such that uncertainty-intolerant individuals experienced greater brain-to-brain synchrony with politically like-minded peers and lower synchrony with political opponents. Third, the neural fingerprint of these uncertainty-modulated polarized perceptions predicted subsequent polarized attitudes outside of the scanner. Taken together, these findings indicate that uncertainty attitudes gate the shared neural processing of political narratives with our political allies and opponents, thereby fueling polarized attitude formation about hot-button issues. Aversion to uncertainty influenced whether the political content was represented similarly in the brain, suggesting that uncertainty-intolerant people see the political world through a stronger partisan lens and construe a more biased picture of the political reality (9, 71). Ideology is not the only driver of polarization: Cognitive traits such as intolerance to uncertainty—which have long been posited to be the lynch pin of political polarization (25)—interact with ideology to form a polarized perception of the world.

Our findings reveal a mechanism by which this polarized perception occurs: neural synchrony. Neural synchrony is a useful and reliable benchmark that two people are interpreting the same

external information in a similar way (36, 45, 72). Individuals who were intolerant to uncertainty and shared the same political beliefs exhibited the greatest brain-to-brain coupling. Evidence of neural synchrony when passively viewing political topics presented with incendiary language, but not during neutrally worded political narratives, reveals that provocative language shapes the rise of polarized perceptions. That these differences emerged in brain regions typically associated with the mentalizing network [i.e., TPJ, precuneus, and DMPFC (54–58)], accords with the idea that political polarization is driven by a lack of shared understanding (65, 70). The ability of two people to have a similar perspective about the content of a complex, abstract, and evolving narrative appears to rest in higher-level processing regions that play a critical role in representing another's beliefs and intentions (36, 39). We also observed that socioemotional and valuation regions, such as the OFC and AI (50, 52, 59–61), exhibited greater neural synchrony in uncertainty-intolerant, committed partisans. This indicates that intensifying partisan animus might stem from divergent emotional experiences that lead to different valuation of the same stimulus. Indeed, the growing animosity between parties—known as affective polarization (70)—is posited to arise from raw and reflexive emotional responding (73, 74).

This work extends recent research on neural polarization in several important ways. Prior work shows that synchrony at the neural level indexes shared political ideology (34), and that ideology can shape even the most basic perceptual processes in detrimental ways (75). Our results suggest that neural polarization may only arise when political information is presented in a polarizing way to uncertainty-averse citizens. Furthermore, prior research has described distinct functional or even structural brain signatures of liberalism and conservatism (76–78). By contrast, our results reveal commonalities in how neural activity is synchronized among opposing ideological groups. This implies that polarized perception is not irreparable but depends on additional factors that vary between stimuli, contexts, and individuals. The growing uncertainty caused by large-scale societal events in the past year (e.g., job loss and a pandemic) may fuel political polarization by sowing rigidly partisan perceptions of the world. Conversely, interventions against polarization may be successful by addressing citizens' sources of worry (20, 79).

Methods

Participants. The data analyzed for this paper were collected as part of a larger study on political preferences. For this study, 360 potential participants completed a screening survey prompted by online advertisements, paper flyers, personal visits to political meetings throughout the state, or word of mouth. The slider measure of ideology (47) was administered in the screening survey. Based on this measure, we invited 22 self-reported conservatives and 22 liberals for an in-laboratory session, all of whom were right handed and eligible for MRI. One participant was excluded from the analysis because they indicated a different ideology on the screening survey versus the postscan political survey battery (see below), leaving 21 conservatives (13 men and 8 women; age range 18 to 61, mean $36 \text{ y} \pm \text{SD } 15 \text{ y}$) and 22 liberals (13 men and 9 women; age range 18 to 60, mean age $28 \pm 12 \text{ y}$). Ideological extremism was computed from the ideology slider measure as $|50 - \text{ideology}|$. The 43 participants represented a range of ideological extremity (Fig. 1C). Neither age nor gender differed significantly between the two groups (all P s > 0.05), but to ensure that our effects were not driven by demographic differences, we controlled for them in several analyses, which confirmed our findings (*SI Appendix, Figs. S5 and S6*; see Control Analyses). The two groups were matched on education level (number of years completed) and annual income (two-sample t tests, two-sided: all P s > 0.4). All participants provided written informed consent and were paid for their participation in the study. The study procedures were approved by the Brown University Institutional Review Board.

Procedure. Participants came to the laboratory for one session of about 3 h. A subset of the tasks was analyzed for the current paper. The first half of the study session took place in the fMRI laboratory. Upon arrival, participants read instructions about the experiment, answered comprehension questions, and confirmed or updated their MRI screening information. Participants then

entered the MRI scanner for a scanning session of about 1.5 h, with soft padding positioned around their head to minimize head motion. In the scanner, participants completed a cognitive task (not analyzed here), underwent a 5-min anatomical scan, and completed the video-watching task described in the main text. During the scans, participants wore two electrodes on their nondominant (left) hand to measure skin conductance. They held a button response box in their right hand. In between each scanner run or task block, the experimenter verbally communicated with the participants to ensure that they were comfortable and attentive. The video watching task consisted of a fixed sequence of three videos, which can be viewed at the following web pages: 1) BBC Earth, "Beaver Lodge Construction Squad" (80); 2) PBS News Hour, "State battles over abortion policy anticipate a post-Roe world" (81); and 3) CNN, "Vice-Presidential Debate 2016" between liberal Democrat Tim Kaine and conservative Republican Mike Pence, clip from about 24:35 to 42:10 (82).

After participants were taken out of the scanner, the experimenter walked with them to a different building on campus for behavioral testing. During this session, participants first completed a survey of their comprehension and judgment of the videos. Judgment items measured attitudes about statements made in the debate video on a seven-point, Likert-type response scale ranging from "Strongly disagree" to "Strongly agree." Next, participants completed several cognitive tasks (not analyzed here) and an extensive survey battery of five political and three cognitive questionnaires. The political questionnaires were the updated Social and Economic Conservatism Scale [SECS (83)], the Schwartz's Short Values Survey [SSVS (84)], Right- (85) and Left-Wing (86) Authoritarianism surveys, and a short-form Social Dominance Orientation survey (87). The cognitive questionnaires were the IUS (21), a short NFC scale (88), and the Interpersonal Reactivity Index (89).

fMRI Acquisition. MRI images were collected on a Siemens Prisma Fit 3-Tesla research-dedicated scanner. T2*-weighted functional scans were acquired using a multislice sequence, capturing three slices at once to ensure whole-brain coverage with short repetition time (repetition time [TR] = 1,500 ms), which increases the number of time points and thus statistical power for brain-to-brain temporal synchrony analysis. A total of 60 3-mm transverse slices were acquired, each with 64×64 voxels 3-mm isotropic, building up a field of view (FOV) that covered the entire brain, except part of the cerebellum. The FOV was tilted upward by 25° at the front of the brain to minimize tissue gradient-related signal dropout in the OFC. Contrast settings were optimized for cortical gray matter (echo time [TE] = 30 ms, flip angle = 86°). T1-weighted (T1w) anatomical scans were acquired using a standard magnetization prepared rapid acquisition gradient echo (MPRAGE) sequence (160 sagittal slices with 256×256 voxels 1-mm isotropic, TR = 1,900 ms, TE = 3.02 ms, flip angle = 9°).

Behavioral Data Preprocessing. As a validation of our ideology measure, a principal component analysis (PCA) on the five political survey measures (SECS, SSVS, etc.) revealed the first component that accounted for 37% of variance across all survey items and was very strongly correlated to the ideology scale measure from the screening survey [$r(41) = 0.89, P < 0.001$]. This strong relationship across time and surveys validates the ideology scale used to recruit participants as a reliable metric of fundamental political orientation. The PCA also identified one participant as a strong outlier, as he had rated his ideology as strongly conservative on the screening slider measure but scored more than three SDs below the mean of the conservative group on the first component of the PCA (in fact, scoring squarely among the liberals); this participant was therefore excluded from analysis.

IUS and NFC item scores were averaged for each participant and normalized to a zero to one range; total scores were multiplied within dyad to obtain joint IUS. Just as individual-level IUS was not associated with ideology (see main text), pairwise ideology similarity was not associated with joint IUS [$r(859) = 0.035, P = 0.30$] nor with pairwise cosine similarity in responses across the entire IUS survey [$r(859) = 0.023, P = 0.50$].

Ideology similarity was computed as $100 - ||$ and then z-scored. Inter-subject agreement about a given video was computed as the cosine similarity between the two participants' ratings.

Behavioral Data Analysis. Throughout this paper, video judgment and neural synchrony data were analyzed using an IS-RSA (44) framework implemented using dyadic regression models. We wrote a custom implementation of the mixed-effects regression approach reported by Chen, Taylor, Shin, Reynolds, and Cox (42) based on the packages *lme4* 1.1-23 and *lmerTest* 3.1-2 for R 3.5.2 (a link to the analysis code can be found under Data Availability). Since each observation in a dyadic regression corresponded to a unique pair of subjects, the model for each observation included a random participant

intercept for both participants involved in that participant pair, which critically accounted for the inherent statistical dependencies between pairwise observations (42, 90). All linear mixed-effects models thus followed the general form:

$$z_{ij} = \gamma + X_{ij}\beta + \alpha_i + \alpha_j + \epsilon_{ij},$$

$$\alpha \sim N(0, \sigma_\alpha),$$

$$\epsilon \sim N(0, \sigma_\epsilon),$$

where i and j represent two participants in a dyad. Duplicate observations of the same dyad were excluded by constraining $i > j$. Pair-wise observations z_{ij} (e.g., similarity between two subjects in ratings of a video) were regressed onto a set of regressors that includes one or more fixed effects X_{ij} (for instance “ideology similarity” or “joint IUS”), random subject intercepts α_i and α_j , and an error term. To compare judgment across videos, we included fixed-effect interactions with a video identity predictor (yielding X_{ijv}), a video main effect γ_v , and random nested video-within-subject intercepts η_{iv} and η_{jv} :

$$z_{ijv} = \gamma_v + X_{ijv}\beta + \alpha_i + \alpha_j + \eta_{iv} + \eta_{jv} + \epsilon_{ijv},$$

$$\alpha \sim N(0, \sigma_\alpha),$$

$$\epsilon \sim N(0, \sigma_\epsilon),$$

$$\eta_v \sim N(0, \sigma_{\eta_v}).$$

fMRI Data Preprocessing. Results included in this manuscript come from preprocessing performed using *fMRIPrep* 1.5.1rc2 [(91) RRID: SCR_016216], which is based on *Nipype* 1.3.0-rc1 [(92, 93) RRID: SCR_002502]. The pipeline description below was copied from the *fMRIPrep* boilerplate text, leaving out unused components.

The T1w image was corrected for intensity nonuniformity with *N4BiasFieldCorrection* (94), distributed with *ANTs* 2.2.0 [(95) RRID: SCR_004757], and used as T1w reference throughout the workflow. The T1w reference was then skull stripped with a *Nipype* implementation of the *antsBrainExtraction.sh* workflow (from *ANTs*), using *OASIS30ANTs* as target template. Brain tissue segmentation of cerebrospinal fluid (CSF), white matter (WM), and gray matter was performed on the brain-extracted T1w using *fast* [(96) FSL 5.0.9, RRID: SCR_002823]. Volume-based spatial normalization to one standard space (*MNI152NLin2009cAsym*) was performed through nonlinear registration with *antsRegistration* (*ANTs* 2.2.0), using brain-extracted versions of both T1w reference and the T1w template. The following template was selected for spatial normalization: *ICBM 152 Nonlinear Asymmetrical template version 2009c* [(97) RRID: SCR_008796; TemplateFlow ID: *MNI152NLin2009cAsym*].

For each of the three BOLD runs per subject, the following preprocessing was performed. First, a reference volume and its skull-stripped version were generated using a custom methodology of *fMRIPrep*. The BOLD reference was then coregistered to the T1w reference using *flirt* [(98) FSL 5.0.9], with the boundary-based registration (99) cost function. Coregistration was configured with 9° of freedom to account for distortions remaining in the BOLD reference. Head-motion parameters with respect to the BOLD reference (transformation matrices and six corresponding rotation and translation parameters) are estimated before any spatiotemporal filtering using *mcflirt* [(100) FSL 5.0.9]. BOLD runs were slice time corrected using *3dTshift* from *AFNI* 20160207 [(101) RRID: SCR_005927]. The BOLD time series (including slice-timing correction when applied) were resampled onto their original, native space by applying a single, composite transform to correct for head-motion and susceptibility distortions. These resampled BOLD time series will be referred to as preprocessed BOLD in original space or just preprocessed BOLD. The BOLD time series were resampled into standard space, generating a preprocessed BOLD run in *MNI152NLin2009cAsym* space. First, a reference volume and its skull-stripped version were generated using a custom methodology of *fMRIPrep*. Several confounding time series were calculated based on the preprocessed BOLD: framewise displacement (FD), the root mean square of the signal after temporal derivation (DVARs), and three region-wise global signals. FD and DVARs are calculated for each functional run, both using their implementations in *Nipype* [following the definitions by Power and colleagues (102)]. The three global signals are extracted within the CSF, the WM, and the whole-brain masks. The head-motion estimates calculated in the correction step were also placed within the corresponding confounds file. The confound time series derived from

head-motion estimates and global signals were expanded with the inclusion of temporal derivatives and quadratic terms for each (103). Frames that exceeded a threshold of 1-mm FD were annotated as motion outliers. Gridded (volumetric) resamplings were performed using *antsApplyTransforms* (*ANTs*), configured with Lanczos interpolation to minimize the smoothing effects of other kernels (104).

For the “Beaver Lodge Construction Squad” video (80), two participants’ data were excluded from analysis, one due to falling asleep in the scanner and one due to excessive head motion. For the “Vice-Presidential Debate 2016” video (82), one participant’s data were excluded from analysis due to excessive head motion. All other functional fMRI data were further preprocessed using *nltools* 0.3.14 (105) to remove signal components related to motion and other sources of noise. To this end, general linear models of each voxel’s signal time series were constructed with the following 29 or more regressors: average CSF signal; average white matter signal; the six realignment parameters, their derivatives, their squares, and their squared derivatives (106); zero-, first-, and second-order polynomials for the removal of intercepts and linear/quadratic trends; and a regressor for each motion spike, which has a value of 1 at the TR where the spike was detected (FD > 1 mm) and zeros elsewhere. The residual time series of each voxel were then used for statistical analysis.

fMRI Data Analysis. We first established that all three videos elicited robust baseline neural synchrony between all participants [known as ISC (33, 40)]. To this end, we followed the ISC procedure used by Leong, Chen, Willer, and Zaki (34): we 1) correlated each participant’s signal time course in a voxel to the average time course of all other participants, 2) subjected the resulting distribution of r values to a sign-flip permutation test (5,000 permutations) to see whether its average value was greater than zero, and 3) thresholded voxel-wise P values at a false-discovery rate (FDR) of 0.001 using the Benjamini–Hochberg method (107).

For the remaining fMRI analyses, which were all IS-RSA (44), we used the mixed-effects dyadic regression method in R described under *Behavioral Data Analysis*. The dependent variable was the z-scored Pearson correlation of the BOLD signal time courses between each pair of subjects for a given voxel.

For the first neural IS-RSA, we regressed this neural synchrony metric onto ideology similarity (defined above). To explore the many activation clusters found in this analysis, refer to the unthresholded beta map on Neurovault (<https://identifiers.org/neurovault.image:453291>). The signal time courses in Fig. 2D were generated from the mean BOLD time series in a spherical ROI with radius = 6 mm centered around the peak voxel for the ideology effect in mOFC.

For the second neural IS-RSA, we regressed neural synchrony onto ideology similarity and joint IUS, the latter of which is the product of both participants’ total IUS scores normalized to a zero to one range. By also including the interaction effect between these two regressors, we could test whether IUS modulated the effect of ideology on brain response. Regressor beta maps were thresholded at FDR-corrected P values of 0.05 using the Benjamini–Hochberg method, as implemented in the *p.adjust* function in R. Surviving clusters were reported if they contained five or more contiguous voxels.

For the region-of-interest analyses in Fig. 3B and C, we first extracted mean activity time courses in each ROI for each participant and computed the brain-to-brain synchrony in these mean signals (“ROI-level neural synchrony”). As ROIs, we used activation clusters from the whole-brain ideology-IUS IS-RSA analysis. The precuneus, TPJ, and OFC ROIs corresponded to our preregistered regions of interest (<https://accounts.osf.io/login?service=https://osf.io/zsjdc/>) and were previously found to process subjective interpretations of narrative content (35). For the estimated effect plots in Fig. 3B, we reran the IS-RSA with ideology similarity (unstandardized), IUS, and their interaction on ROI-level neural synchrony. We then used the effect estimates from the fitted mixed-effects regression models to simulate the dependent variable (neural synchrony) at a dense grid of ideology similarity and joint-IUS values, whose axis limits matched those observed in the dataset. For the line plots in Fig. 3C, we estimated marginal effects of ideology similarity on brain-to-brain synchrony at the first quartile and third quartile of the joint IUS distribution.

For the ANCOVA, we ran our dyadic regression model of neural synchrony with a categorical predictor “ideology pair” with three levels, which indicated whether a dyad contained two conservatives (CC), two liberals (LL), or CL (baseline). For the post hoc pairwise comparisons, we again extracted ROI-level neural synchrony from the 19 active clusters and ran the ANCOVA for each ROI, using the contrast function from *emmeans* 1.5.4 in R to obtain post hoc comparisons of the slope of joint IUS under treatment (CC or LL) versus baseline (CL), which adjusts P values using Dunnett’s method (108).

For the analysis using neural synchrony to predict judgment similarity, ROI-wise neural synchrony was computed by correlating the mean activity time

courses from a given activation cluster (defined at the group level) between each pair of subjects. This ROI-wise neural similarity metric was then used as a predictor in a dyadic regression model of judgment similarity defined as described above.

Control Analyses. It is well established that similarities on demographic and social variables can increase intersubject synchrony in brain responses to video stimuli (90). Although this potential confound cannot account for the ideology-IUS interaction effects that were observed in our key analyses, we nevertheless wanted to ensure that the effects reported here were specific to political polarization. To this end, we reran the IS-RSA analyses with additional regressors, each controlling for a demographic or experimental factor that may impact neural synchrony: age, gender, undergraduate student status, sampling source (from the university or from the community), and scan day (participants were scanned across a ~6-mo period). For the ideology model, no clusters survived this additional control for the “State battles over abortion policy anticipate a post-Roe world” video (81) but nearly all of the many active clusters survived for the “Vice-Presidential

Debate 2016” video (82) (SI Appendix, Fig. S5). For the ideology-IUS interaction model, all clusters survived except the precuneus (SI Appendix, Fig. S6).

Data Availability. All analysis code needed to reproduce the results in this paper is available on GitHub (https://github.com/jeroenvanbaar/PNAS_uncertainty_polarization). Source data is available from the authors upon reasonable request.

ACKNOWLEDGMENTS. This work was supported by the Brown University Office of the Vice President for Research Seed Fund Award GR300152 and NIH Centers of Biomedical Research Excellence grant P20GM103645. We thank Uri Hasson for fruitful discussions during study design and analysis. We are grateful to Pedro Rodriguez, Daantje de Bruin, and members of the FeldmanHall Laboratory for productive conversations on study design. We thank Wenning Deng, Marlon Sherman, Rachel Yan, Logan Bickel, Avinash Vaidya, Romy Froemer, Amrita Lamba, Lynn Fanella, and Fabienne McEleney for helping us with data collection.

1. E. J. Finkel, et al., Political sectarianism in America. *Science* **370**, 533–536 (2020).
2. S. Iyengar, S. J. Westwood, Fear and loathing across party lines: New evidence on group polarization. *Am. J. Pol. Sci.* **59**, 690–707 (2015).
3. D. Baldassarri, A. Gelman, Partisans without constraint: Political polarization and trends in American public opinion. *AJS* **114**, 408–446 (2008).
4. J. M. van Baar, O. FeldmanHall, The polarized mind in context: Interdisciplinary approaches to the psychology of political polarization. *Am. Psychol.*, 10.1037/amp0000814 (2021).
5. M. Somer, J. McCoy, Déjà vu? Polarization and endangered democracies in the 21st century. *Am. Behav. Sci.* **62**, 3–15 (2018).
6. R. P. Vallone, L. Ross, M. R. Lepper, The hostile media phenomenon: Biased perception and perceptions of media bias in coverage of the Beirut massacre. *J. Pers. Soc. Psychol.* **49**, 577–585 (1985).
7. C. G. Lord, L. Ross, M. R. Lepper, Biased assimilation and attitude polarization: The effects of prior theories on subsequently considered evidence. *J. Pers. Soc. Psychol.* **37**, 2098–2109 (1979).
8. D. M. Kahan, D. A. Hoffman, D. Braman, D. Evans, J. J. Rachlinski, “They saw a protest”: Cognitive illiberalism and the speech-conduct distinction. *Stanford Law Rev.* **64**, 851–906 (2012).
9. A. Alesina, A. Miano, S. Stantcheva, The polarization of reality. *AEA Pap. Proc.* **110**, 324–328 (2020).
10. K. M. Klein, A. W. Kruglanski, Commitment and extremism: A goal systemic analysis. *J. Soc. Issues* **69**, 419–435 (2013).
11. L. Zmigrod, The role of cognitive rigidity in political ideologies: Theory, evidence, and future directions. *Curr. Opin. Behav. Sci.* **34**, 34–39 (2020).
12. M. Kemmelmeier, Political conservatism, rigidity, and dogmatism in American foreign policy officials: The 1966 Mennis data. *J. Psychol.* **141**, 77–90 (2007).
13. J.-W. van Prooijen, A. P. M. Krouwel, Psychological features of extreme political ideologies. *Curr. Dir. Psychol. Sci.* **28**, 159–163 (2019).
14. D. M. Webster, A. W. Kruglanski, Individual differences in need for cognitive closure. *J. Pers. Soc. Psychol.* **67**, 1049–1062 (1994).
15. H. Eysenck, *The Psychology of Politics* (Routledge, 1998).
16. J. T. Jost, Ideological asymmetries and the essence of political psychology. *Polit. Psychol.* **38**, 167–208 (2017).
17. L. Zmigrod, P. J. Rentfrow, T. W. Robbins, The partisan mind: Is extreme political partisanship related to cognitive inflexibility? *J. Exp. Psychol. Gen.* **149**, 407–418 (2020).
18. J. Greenberg, E. Jonas, Psychological motives and political orientation—the left, the right, and the rigid: Comment on Jost et al. (2003). *Psychol. Bull.* **129**, 376–382, discussion 383–393 (2003).
19. P. M. Fernbach, T. Rogers, C. R. Fox, S. A. Sloman, Political extremism is supported by an illusion of understanding. *Psychol. Sci.* **24**, 939–946 (2013).
20. M. H. Freeston, J. Rhéaume, H. Letarte, M. J. Dugas, R. Ladouceur, Why do people worry? *Pers. Individ. Differ.* **17**, 791–802 (1994).
21. K. Buhr, M. J. Dugas, The intolerance of uncertainty scale: Psychometric properties of the English version. *Behav. Res. Ther.* **40**, 931–945 (2002).
22. T. W. Adorno, E. Frenkel-Brunswick, D. J. Levinson, R. N. Sanford, *The Authoritarian Personality* (Harper Brothers, 1950).
23. R. M. Alvarez, C. H. Franklin, Uncertainty and political perceptions. *J. Polit.* **56**, 671–688 (1994).
24. A. Downs, An economic theory of political action in a democracy. *J. Polit. Econ.* **65**, 135–150 (1957).
25. E. Frenkel-Brunswick, Intolerance of ambiguity as an emotional and perceptual personality variable. *J. Pers.* **18**, 108–143 (1949).
26. E. Hoffer, *The True Believer: Thoughts On the Nature of Mass Movements* (Harper & Brothers, 1951).
27. K. M. McGraw, E. Hasecke, K. Conger, Ambivalence, uncertainty, and processes of candidate evaluation. *Polit. Psychol.* **24**, 421–448 (2003).
28. I. J. Haas, M. N. Baker, F. J. Gonzalez, Political uncertainty moderates neural evaluation of incongruent policy positions. *Philos. Trans. R. Soc. Lond. B Biol. Sci.* **376**, 20200138 (2021).
29. I. J. Haas, W. A. Cunningham, The uncertainty paradox: Perceived threat moderates the effect of uncertainty on political tolerance. *Polit. Psychol.* **35**, 291–302 (2014).
30. J. T. Jost, J. Glaser, A. W. Kruglanski, F. J. Sulloway, Political conservatism as motivated social cognition. *Psychol. Bull.* **129**, 339–375 (2003).
31. J. T. Jost, D. M. Amodio, Political ideology as motivated social cognition: Behavioral and neuroscientific evidence. *Motiv. Emot.* **36**, 55–64 (2012).
32. M. A. Hogg, Uncertainty-identity theory. *Adv. Exp. Soc. Psychol.* **39**, 69–126 (2007).
33. U. Hasson, Y. Nir, I. Levy, G. Fuhrmann, R. Malach, Intersubject synchronization of cortical activity during natural vision. *Science* **303**, 1634–1640 (2004).
34. Y. C. Leong, J. Chen, R. Willer, J. Zaki, Conservative and liberal attitudes drive polarized neural responses to political content. *Proc. Natl. Acad. Sci. U.S.A.* **117**, 27731–27739 (2020).
35. Y. Yeshurun et al., Same story, different story. *Psychol. Sci.* **28**, 307–319 (2017).
36. U. Hasson, A. A. Ghazanfar, B. Galantucci, S. Garrod, C. Keysers, Brain-to-brain coupling: A mechanism for creating and sharing a social world. *Trends Cognit. Sci.* **16**, 114–121 (2012).
37. T. Wheatley, O. Kang, C. Parkinson, C. E. Looser, From mind perception to mental connection: Synchrony as a mechanism for social understanding. *Soc. Personal. Psychol. Compass* **6**, 589–606 (2012).
38. G. R. Semin, “Grounding communication: Synchrony” in *Social Psychology: Handbook of Basic Principles*, A. W. Kruglanski, E. T. Higgins, Eds. (The Guilford Press, 2007), pp. 630–649.
39. A. Stolk, L. Verhagen, I. Toni, Conceptual alignment: How brains achieve mutual understanding. *Trends Cognit. Sci.* **20**, 180–191 (2016).
40. S. A. Nastase, V. Gazzola, U. Hasson, C. Keysers, Measuring shared responses across subjects using intersubject correlation. *Soc. Cognit. Affect Neurosci.* **14**, 667–685 (2019).
41. B. F. Schaffner, S. Luks, Misinformation or expressive responding? What an inauguration crowd can tell us about the source of political misinformation in surveys. *Publ. Opin. Q.* **82**, 135–147 (2018).
42. G. Chen, P. A. Taylor, Y.-W. Shin, R. C. Reynolds, R. W. Cox, Untangling the relatedness among correlations, Part II: Inter-subject correlation group analysis through linear mixed-effects modeling. *Neuroimage* **147**, 825–840 (2017).
43. E. S. Finn et al., Idiosynchrony: From shared responses to individual differences during naturalistic neuroimaging. *Neuroimage* **215**, 116828 (2020).
44. J. M. van Baar, L. J. Chang, A. G. Sanfey, The computational and neural substrates of moral strategies in social decision-making. *Nat. Commun.* **10**, 1483 (2019).
45. M. Nguyen, T. Vanderwal, U. Hasson, Shared understanding of narratives is correlated with shared neural responses. *Neuroimage* **184**, 161–170 (2019).
46. G. J. Stephens, L. J. Silbert, U. Hasson, Speaker-listener neural coupling underlies successful communication. *Proc. Natl. Acad. Sci. U.S.A.* **107**, 14425–14430 (2010).
47. M. D. Dodd et al., The political left rolls with the good and the political right confronts the bad: Connecting physiology and cognition to preferences. *Philos. Trans. R. Soc. Lond. B Biol. Sci.* **367**, 640–649 (2012).
48. N. Kriegeskorte, M. Mur, P. Bandettini, Representational similarity analysis - connecting the branches of systems neuroscience. *Front. Syst. Neurosci.* **2**, 4 (2008).
49. O. Bartra, J. T. McGuire, J. W. Kable, The valuation system: A coordinate-based meta-analysis of BOLD fMRI experiments examining neural correlates of subjective value. *Neuroimage* **76**, 412–427 (2013).
50. J. O’Doherty, M. L. Krangelbach, E. T. Rolls, J. Hornak, C. Andrews, Abstract reward and punishment representations in the human orbitofrontal cortex. *Nat. Neurosci.* **4**, 95–102 (2001).
51. F. Van Overwalle, K. Baetens, Understanding others’ actions and goals by mirror and mentalizing systems: A meta-analysis. *Neuroimage* **48**, 564–584 (2009).
52. L. J. Chang, T. Yarkoni, M. W. Khaw, A. G. Sanfey, Decoding the role of the insula in human cognition: Functional parcellation and large-scale reverse inference. *Cerebr. Cortex* **23**, 739–749 (2013).
53. E. T. Rolls, The orbitofrontal cortex and reward. *Cerebr. Cortex* **10**, 284–294 (2000).
54. L. Tsoi, J. Dungan, A. Waytz, L. Young, Distinct neural patterns of social cognition for cooperation versus competition. *Neuroimage* **137**, 86–96 (2016).
55. A. E. Skerry, R. Saxe, Neural representations of emotion are organized around abstract event features. *Curr. Biol.* **25**, 1945–1954 (2015).

56. R. Saxe, Uniquely human social cognition. *Curr. Opin. Neurobiol.* **16**, 235–239 (2006).
57. J. Koster-Hale, R. Saxe, J. Dungan, L. L. Young, Decoding moral judgments from neural representations of intentions. *Proc. Natl. Acad. Sci. U.S.A.* **110**, 5648–5653 (2013).
58. R. A. Mar, The neural bases of social cognition and story comprehension. *Annu. Rev. Psychol.* **62**, 103–134 (2011).
59. A. Bechara, H. Damasio, A. R. Damasio, Emotion, decision making and the orbitofrontal cortex. *Cerebr. Cortex* **10**, 295–307 (2000).
60. J. Zaki, J. I. Davis, K. N. Ochsner, Overlapping activity in anterior insula during interoception and emotional experience. *Neuroimage* **62**, 493–499 (2012).
61. A. D. B. Craig, How do you feel—now? The anterior insula and human awareness. *Nat. Rev. Neurosci.* **10**, 59–70 (2009).
62. D. Schmuck, M. Tribastone, J. Matthes, F. Marquart, E. M. Bergel, Avoiding the other side? An eye-tracking study of selective exposure and selective avoidance effects in response to political advertising. *J. Media Psychol.* **32**, 158–164 (2020).
63. H. Tajfel, Social identity and intergroup behaviour. *Soc. Sci. Inf.* **13**, 65–93 (1974).
64. H. Tajfel, J. Turner, "An integrative theory of intergroup conflict" in *The Social Psychology of Intergroup Relations*, W. G. Austin, S. Worchel, Eds. (Brooks/Cole, 1979), pp. 33–47.
65. S. Iyengar, M. Krupenkin, The strengthening of partisan affect. *Polit. Psychol.* **39**, 201–218 (2018).
66. L. Mason, Ideologues without issues: The polarizing consequences of ideological identities. *Publ. Opin. Q.* **82**, 866–887 (2018).
67. J. J. Van Bavel, A. Pereira, The partisan brain: An identity-based model of political belief. *Trends Cognit. Sci.* **22**, 213–224 (2018).
68. J. Lees, M. Cikara, Inaccurate group meta-perceptions drive negative out-group attributions in competitive intergroup contexts. *Nat. Hum. Behav.* **4**, 279–286 (2020).
69. A. Waytz, L. L. Young, J. Ginges, Motive attribution asymmetry for love vs. hate drives intractable conflict. *Proc. Natl. Acad. Sci. U.S.A.* **111**, 15687–15692 (2014).
70. S. Iyengar, Y. Leikes, M. Levendusky, N. Malhotra, S. J. Westwood, The origins and consequences of affective polarization in the United States. *Annu. Rev. Polit. Sci.* **22**, 129–146 (2019).
71. A. H. Hastorf, H. Cantril, They saw a game: A case study. *J. Abnorm. Psychol.* **49**, 129–134 (1954).
72. A. Stolk *et al.*, Cerebral coherence between communicators marks the emergence of meaning. *Proc. Natl. Acad. Sci. U.S.A.* **111**, 18183–18188 (2014).
73. Y. Leikes, G. Sood, S. Iyengar, The hostile audience: The effect of access to broadband internet on partisan affect. *Am. J. Pol. Sci.* **61**, 5–20 (2017).
74. L. Huddy, L. Mason, L. Aarøe, Expressive partisanship: Campaign involvement, political emotion, and partisan identity. *Am. Polit. Sci. Rev.* **109**, 1–17 (2015).
75. E. M. Caruso, N. L. Mead, E. Balcetis, Political partisanship influences perception of biracial candidates' skin tone. *Proc. Natl. Acad. Sci. U.S.A.* **106**, 20168–20173 (2009).
76. R. Kanai, T. Feilden, C. Firth, G. Rees, Political orientations are correlated with brain structure in young adults. *Curr. Biol.* **21**, 677–680 (2011).
77. D. Schreiber *et al.*, Red brain, blue brain: Evaluative processes differ in democrats and republicans. *PLoS One* **8**, e52970 (2013).
78. W.-Y. Ahn *et al.*, Nonpolitical images evoke neural predictors of political ideology. *Curr. Biol.* **24**, 2693–2699 (2014).
79. A. Lamba, M. J. Frank, O. FeldmanHall, Anxiety impedes adaptive social learning under uncertainty. *Psychol. Sci.* **31**, 592–603 (2020).
80. BBC Earth, "Beaver Lodge Construction Squad | Attenborough | BBC Earth" (video recording, 2009). <https://www.youtube.com/watch?v=iyNA62FrKCE>. Accessed 6 May 2021.
81. Public Broadcasting Service, "State battles over abortion policy anticipate a post-Roe world" (video recording, 2019). <https://www.pbs.org/newshour/show/state-battles-over-abortion-policy-anticipate-a-post-roe-world>. Accessed 6 May 2021.
82. Cable News Network, "Entire vice presidential debate: Pence vs. Kaine" (video recording, 2016). <https://www.youtube.com/watch?v=ox8PTXwDYdc>. Accessed 6 May 2021.
83. J. A. C. Everett, The 12 item social and economic conservatism scale (SECS). *PLoS One* **8**, e82131 (2013).
84. M. Lindeman, M. Verkasalo, Measuring values with the Short Schwartz's Value Survey. *J. Pers. Assess.* **85**, 170–178 (2005).
85. F. Funke, The dimensionality of right-wing authoritarianism: lessons from the dilemma between theory and measurement. *Polit. Psych.* **26**, 195–218 (2005).
86. L. G. Conway III, S. C. Houck, L. J. Gornick, M. A. Repke, Finding the Loch Ness monster: Left-wing authoritarianism in the United States. *Polit. Psychol.* **39**, 1049–1067 (2018).
87. A. K. Ho *et al.*, The nature of social dominance orientation: Theorizing and measuring preferences for intergroup inequality using the new SDO₇ scale. *J. Pers. Soc. Psychol.* **109**, 1003–1028 (2015).
88. A. Roets, A. Van Hiel, Item selection and validation of a brief, 15-item version of the Need for Closure Scale. *Pers. Individ. Differ.* **50**, 90–94 (2011).
89. M. H. Davis, Measuring individual differences in empathy: Evidence for a multidimensional approach. *J. Pers. Soc. Psychol.* **44**, 113–126 (1983).
90. C. Parkinson, A. M. Kleinbaum, T. Wheatley, Similar neural responses predict friendship. *Nat. Commun.* **9**, 332 (2018).
91. O. Esteban *et al.*, fMRIPrep: A robust preprocessing pipeline for functional MRI. *Nat. Methods* **16**, 111–116 (2019).
92. K. Gorgolewski *et al.*, Nipype: A flexible, lightweight and extensible neuroimaging data processing framework in python. *Front. Neuroinf.* **5**, 13 (2011).
93. O. Esteban *et al.*, nipype/nipype: 1.3.0-rc1 (2019). <https://www.doi.org/10.5281/ZENODO.3476537>. Accessed 6 May 2021.
94. N. J. Tustison *et al.*, N4ITK: Improved N3 bias correction. *IEEE Trans. Med. Imaging.* **29**, 1310–1320 (2010).
95. B. B. Avants, C. L. Epstein, M. Grossman, J. C. Gee, Symmetric diffeomorphic image registration with cross-correlation: Evaluating automated labeling of elderly and neurodegenerative brain. *Med. Image Anal.* **12**, 26–41 (2008).
96. Y. Zhang, M. Brady, S. Smith, Segmentation of brain MR images through a hidden Markov random field model and the expectation-maximization algorithm. *IEEE Trans. Med. Imaging.* **20**, 45–57 (2001).
97. V. Fonov, A. Evans, R. McKinstry, C. Almlí, D. Collins, Unbiased nonlinear average age-appropriate brain templates from birth to adulthood. *Neuroimage* **47**, S102 (2009).
98. M. Jenkinson, S. Smith, A global optimisation method for robust affine registration of brain images. *Med. Image Anal.* **5**, 143–156 (2001).
99. D. N. Greve, B. Fischl, Accurate and robust brain image alignment using boundary-based registration. *Neuroimage* **48**, 63–72 (2009).
100. M. Jenkinson, P. Bannister, M. Brady, S. Smith, Improved optimization for the robust and accurate linear registration and motion correction of brain images. *Neuroimage* **17**, 825–841 (2002).
101. R. W. Cox, J. S. Hyde, Software tools for analysis and visualization of fMRI data. *NMR Biomed.* **10**, 171–178 (1997).
102. J. D. Power *et al.*, Methods to detect, characterize, and remove motion artifact in resting state fMRI. *Neuroimage* **84**, 320–341 (2014).
103. T. D. Satterthwaite *et al.*, An improved framework for confound regression and filtering for control of motion artifact in the preprocessing of resting-state functional connectivity data. *Neuroimage* **64**, 240–256 (2013).
104. C. Lanczos, Evaluation of noisy data. *J. Soc. Ind. Appl. Math. Ser. B Numer. Anal.* **1**, 76–85 (1964).
105. L. Chang *et al.*, cosanlab/nltools: 0.3.14 (2019). <https://www.doi.org/10.5281/ZENODO.3251172>. Accessed 6 May 2021.
106. K. J. Friston, S. Williams, R. Howard, R. S. Frackowiak, R. Turner, Movement-related effects in fMRI time-series. *Magn. Reson. Med.* **35**, 346–355 (1996).
107. Y. Benjamini, Y. Hochberg, Controlling the false discovery rate: A practical and powerful approach to multiple testing. *J. Roy. Stat. Soc. B* **57**, 289–300 (1995).
108. C. W. Dunnett, A multiple comparison procedure for comparing several treatments with a control. *J. Am. Stat. Assoc.* **50**, 1096–1121 (1955).